




# High-Power, Narrow-Linewidth Distributed-Feedback Quantum-Cascade Laser for Molecular Spectroscopy

## Journal Article

### Author(s):

[Bertrand, Mathieu](#) ; [Shlykov, Aleksandr](#); [Shahmohamadi, Mehran](#); [Beck, Mattias](#) ; [Willitsch, Stefan](#); [Faist, Jérôme](#) 

### Publication date:

2022-08

### Permanent link:

<https://doi.org/10.3929/ethz-b-000568711>

### Rights / license:

[Creative Commons Attribution 4.0 International](#)

### Originally published in:

Photonics 9(8), <https://doi.org/10.3390/photonics9080589>

### Funding acknowledgement:

183579 - Precision molecular spectroscopy using a network for distribution of the Swiss primary frequency standard (SNF)

## Article

# High-Power, Narrow-Linewidth Distributed-Feedback Quantum-Cascade Laser for Molecular Spectroscopy

Mathieu Bertrand <sup>1,\*</sup>, Aleksandr Shlykov <sup>2</sup>, Mehran Shahmohamadi <sup>1</sup>, Mattias Beck <sup>1</sup>, Stefan Willitsch <sup>2</sup> and Jérôme Faist <sup>1</sup>

<sup>1</sup> Institute for Quantum Electronics, ETH Zurich, 8093 Zurich, Switzerland

<sup>2</sup> Department of Chemistry, University of Basel, 4056 Basel, Switzerland

\* Correspondence: mbertrand@phys.ethz.ch

**Abstract:** Quantum cascade lasers are versatile light sources in the mid-infrared range for molecular spectroscopy which find a wide range of applications from high-resolution studies to sensing. While devices with either high power or narrow spectral linewidth have previously been reported, there is still a lack of sources combining both of these characteristics which are particularly important for precision measurements of weak spectroscopic transitions. In this article, we describe and characterize a novel master-oscillator power-amplifier distributed-feedback quantum cascade laser designed to fill this gap. At an output power of 300 mW, the device features a free-running linewidth of 1.3 MHz, measured with a frequency discriminator technique, at an emission wavenumber of 2185 cm<sup>-1</sup>. This linewidth is sufficiently narrow to enable a further reduction by a tight lock to a high-Q oscillator.

**Keywords:** QCL; linewidth; spectroscopy



**Citation:** Bertrand, M.; Shlykov, A.; Shahmohamadi, M.; Beck, M.; Willitsch, S.; Faist J. High-Power, Narrow-Linewidth Distributed-Feedback Quantum-Cascade Laser for Molecular Spectroscopy. *Photonics* **2022**, *9*, 589. <https://doi.org/10.3390/photonics9080589>

Received: 15 July 2022

Accepted: 12 August 2022

Published: 19 August 2022

**Publisher's Note:** MDPI stays neutral with regard to jurisdictional claims in published maps and institutional affiliations.



**Copyright:** © 2022 by the authors. Licensee MDPI, Basel, Switzerland. This article is an open access article distributed under the terms and conditions of the Creative Commons Attribution (CC BY) license (<https://creativecommons.org/licenses/by/4.0/>).

## 1. Introduction

In recent years, Quantum Cascade Lasers (QCLs) [1] have emerged as leading semiconductor laser sources in the mid-infrared (IR) part of the spectrum from 3 μm to >14 μm. Because numerous molecular rovibrational transitions occupy this spectral region, narrow linewidth QCLs are a key element for mid-IR spectroscopic applications such as high-resolution measurements [2], sensitive detection of molecular gases [3] or high-resolution heterodyne astronomy [4]. Recently, it was shown [5] that it is possible to drive weak dipole-forbidden vibrational transitions with tightly-focused high-power QCLs. However, the broad linewidth of the previously employed laser sources [5] led to significant broadening of these originally extremely narrow transitions. This problem could be solved by implementing a tight lock of the laser to achieve a further linewidth reduction, for instance using a non-linear frequency conversion to the near-IR and referencing to the near-IR frequency comb [6]. Nevertheless, the free-running linewidth of the laser needs to be sufficiently narrow for this technique to be amenable. While a range of either narrow-linewidth [7,8] or high-power QCLs [9–11] have been reported, only a few of them possess both features, which are required for applications such as high-resolution spectroscopy of extremely weak molecular transitions. In general, the phase noise of a laser, responsible for the linewidth of its emission, is ultimately limited by the spontaneous emission that continuously adds a random perturbation to the optical phase [12]. For semiconductor lasers, the Schawlow–Townes laser linewidth that arises from this noise has to be multiplied by  $1 + \alpha^2$  where the linewidth enhancement factor  $\alpha$  takes into account the conversion of the amplitude noise into phase noise [13]. Because QCLs operate at relatively high optical power, use cavities with relatively low optical losses and exhibit low linewidth enhancement factors  $\alpha < 1$  [14,15], they can exhibit frequency noise limited by the modified Schawlow–Townes limit [8,16]. At low frequencies, typically below 10 MHz, the phase noise generally has a  $1/f^n$  power law scaling which has been attributed to environmental fluctuations including charge-carrier noise [17].

Here, we report the development and characterisation of a high-power narrow-linewidth mid-IR QCL emitting at  $4.56\ \mu\text{m}$  tailored for the spectroscopy of extremely weak, dipole-forbidden molecular transitions in the mid-IR [5,18]. The manufacturing approach using a master-oscillator power-amplifier (MOPA) design [19,20] allowed us to produce more than 300 mW output power. We characterised the linewidth of the laser by the frequency discriminator technique [7] using a spectroscopic transition at  $2185.53\ \text{cm}^{-1}$  in  $\text{N}_2\text{O}$  gas.

## 2. Methods

### 2.1. Manufacturing

The QCL active region designed for this experiment consists of a strain-compensated  $\text{In}_{0.684}\text{Ga}_{0.316}\text{As}/\text{Al}_{0.665}\text{In}_{0.335}\text{As}$  heterogeneous stack of two bound-to-continuum [21] active regions centered respectively at  $2170\ \text{cm}^{-1}$  and  $2325\ \text{cm}^{-1}$ , grown by molecular-beam epitaxy. This peculiar stack configuration was designed and tailored for broad gain allowing the fabrication of lasers over a wider wavelength range. The design of the active region is depicted in Figure 1a where the upper and lower levels of the lasing transition have been colored in orange and blue, respectively.

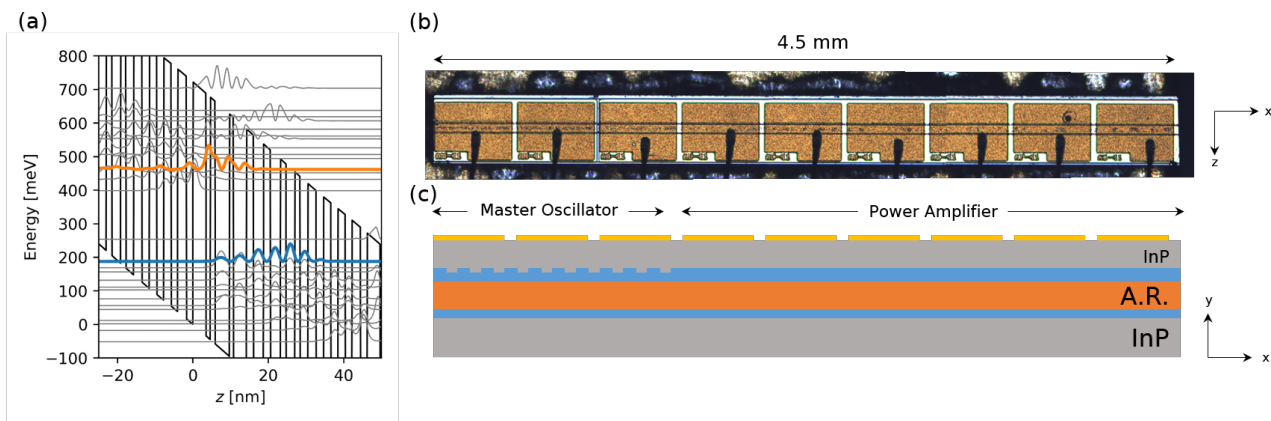


**Figure 1.** (a) One period of the QCL active region together with the computed wavefunctions (grey). The wavefunctions of the upper and lower level of the lasing transitions occurring in this device are highlighted in orange and blue, respectively. (b) Top-view photograph of the device. (c) Schematic (not to scale) of the cross section of the device where the active region (AR), guiding layer, top-contact and InP are respectively colored in orange, blue, gold, and grey.

The MOPA device was processed into narrow ( $5\ \mu\text{m}$  wide), planarized buried-heterostructure waveguides that provide a combination of low lateral waveguides loss and good heat extraction [22,23]. The overall length of the laser is 4.5 mm from which 1/3 of the total length consists of distributed-feedback Bragg (DFB) reflectors centered at  $2190\ \text{cm}^{-1}$ . The remaining 2/3 are the amplifying sections of the device. Figure 1b shows a photograph in top view of the laser after mounting. Figure 1c depicts a schematic of the device cross section (not to scale) with the active region (AR) in orange and the DFB reflectors etched in the guiding InGaAs layer (blue). The front facet of the device was left as cleaved and, to further enhance the output power, a highly reflective coating consisting of 250 nm of  $\text{Al}_2\text{O}_3$  and 350 nm of Au has been deposited on the back facet of the device, resulting in an increase of power of 20%. The electrical pads of the device are connected to the same point, meaning both sections of the device are biased equivalently.

Figure 2a shows the measured light-current (L-I) profile in the continuous-wave (CW) regime for operating temperatures from  $-20\ ^\circ\text{C}$  to  $20\ ^\circ\text{C}$  in steps of  $10\ ^\circ\text{C}$ . The device shows a high output power ( $>300\ \text{mW}$ ) at a working temperature of  $-20\ ^\circ\text{C}$ . The abrupt changes in the profiles at temperatures of  $-20\ ^\circ\text{C}$ ,  $-10\ ^\circ\text{C}$  and  $+20\ ^\circ\text{C}$  are due to hops of the longitudinal mode of the device. Alongside the L-I characterization, the emission spectrum of the laser has been recorded over this temperature range using a commercial Fourier-transform infrared spectrometer (Bruker VERTEX 80). Figure 2b presents the summary

of the measured spectra as a function of the current and the operating temperature of the device. The color map indicates the wavenumber difference  $\Delta\nu = \nu_{laser} - \nu_{ref}$  with  $\nu_{ref} = 2185.53 \text{ cm}^{-1}$  as the chosen reference transition of  $\text{N}_2\text{O}$ . As a guideline, the isoline  $\Delta\nu = 0$  (black trace) gives the operation points in the temperature and current required to measure the linewidth of the laser with the chosen transition. To illustrate the single-mode operation of the device, Figure 2c shows the spectrum recorded at a temperature of  $-20^\circ\text{C}$  for a current of 650 mA. The device features an excellent side-mode-suppression ratio (SMSR) of 40 dB. The unpublished linewidth enhancement factor  $\alpha$  of this device for the operation point shown in Figure 2c) was measured using an RF modulation to be  $\alpha = 0.5$  [24]. With an output power of 320 mW and total losses of  $3.9 \text{ cm}^{-1}$ , this yields to a theoretical Schawlow–Townes limited linewidth of 13.3 Hz.

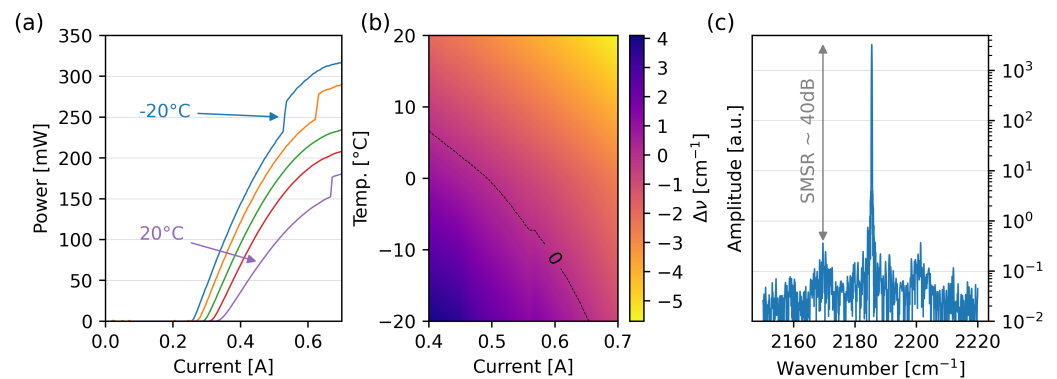


**Figure 2.** (a) Light–current (L–I) curves of the present QCL for temperatures between  $-20^\circ\text{C}$  and  $20^\circ\text{C}$  in increments of  $10^\circ\text{C}$ . (b) Spectral tunability map of the device as a function of current and temperature. The color map indicates the wavenumber difference to a reference spectroscopic transition in  $\text{N}_2\text{O}$  at  $2185.53 \text{ cm}^{-1}$  represented by the dashed line. (c) Spectrum recorded for a temperature of  $-20^\circ\text{C}$  and a current of 650 mA showing a side-mode-suppression ratio (SMSR) of  $\sim 40 \text{ dB}$ .

### 2.2. Characterization

The laser linewidth can be measured using interferometric self-heterodyning [25] or self-homodyning [26] techniques or by direct comparison with a reference narrow-linewidth laser source [27]. However, the self-mixing techniques are inherently limited and cannot be used to measure sub-kHz linewidth. Furthermore, the third technique requires a narrow linewidth device as a reference in the same spectral range as the laser to be measured. In addition, these techniques do not allow us to retrieve the origin of the noise responsible for the broadening of the linewidth. Instead, one can measure the laser frequency noise using the frequency-discriminator technique [7] and calculate the linewidth from the noise obtained [28].

The frequency discriminator technique allows the conversion of the laser frequency noise into amplitude noise using the frequency-dependent transmission through a high-Q Fabry–Perot resonator or a gas cell near a molecular resonance. By calculating the power noise spectral density from the transmitted signal and using the slope of the discriminator to convert amplitude fluctuations into frequency fluctuations, the laser frequency noise in the form of a frequency-noise power spectral density (FNPSD) is obtained. All the noise contributions are separated in two regions delimited by the beta-separation line, determined by [29]:

$$\beta = 8 \ln 2f / \pi^2, \tag{1}$$

where  $f$  is the Fourier frequency. The two regions define a slow-modulation area affecting the laser lineshape and a rapid-modulation area affecting only the wings of the lineshape, respectively. This method allows the estimation of the linewidth of the laser with relatively

high precision from the integral  $A$  of the FNPSD in the slow-modulation region according to [28]:

$$FWHM = \sqrt{8 \ln(2)A}. \tag{2}$$

In our experiment, we measured the transmittance of the IR radiation through a gas cell with a length of 10 cm filled with N<sub>2</sub>O seeded in N<sub>2</sub> at 45 mbar total pressure as a function of time of the QCL laser operating near 2185.53 cm<sup>-1</sup>. The operation current and temperature were set to 650 mA and -20 °C to address the absorption line of interest in the high-power regime. At the seeding ratios of 5–10% N<sub>2</sub>O in N<sub>2</sub> and at the experimental conditions employed in the present study, the theoretical pressure-broadened linewidth of the discriminator line as predicted by the HITRAN database [30] varies approximately between 350 and 440 MHz. The intensity of the radiation transmitted through the cell was measured with an infrared-sensitive HgCdTe photodetector (PVI-4TE-5, Vigo, Ożarów Mazowiecki, Poland) using a transimpedance DC-coupled 10 MHz bandwidth preamplifier (AIP-DC-10M-S, Vigo, Ożarów Mazowiecki, Poland) with a noise floor of 1.56 × 10<sup>-13</sup> V<sup>2</sup>/Hz at 100 kHz. Additionally, the laser beam was split into three branches: one towards the gas cell and one towards a wavemeter and powermeter as depicted in Figure 3a). The low-noise current driver (QubeCL15, ppqSense, Sesto Fiorentino FI, Italy) was modulated using a triangular waveform from a frequency generator (TG200, TTi, Thurlby Thandar Instruments, England) resulting in a modulation of the output frequency of the laser of 3.4 GHz. This modulation was applied to locate the absorption lines in N<sub>2</sub>O on the oscilloscope for selecting the appropriate discriminator line. After measuring the lineshape of the target transition, the modulation was turned off, the laser operation point was set to the center of the discriminator slope and the device was left running freely. For the selected transition, the sensitivity of the transmitted signal-to-frequency fluctuations as extracted from a linear fit to the slope of the lineshape (black line in Figure 3b) amounted to 1.13 mV/MHz.

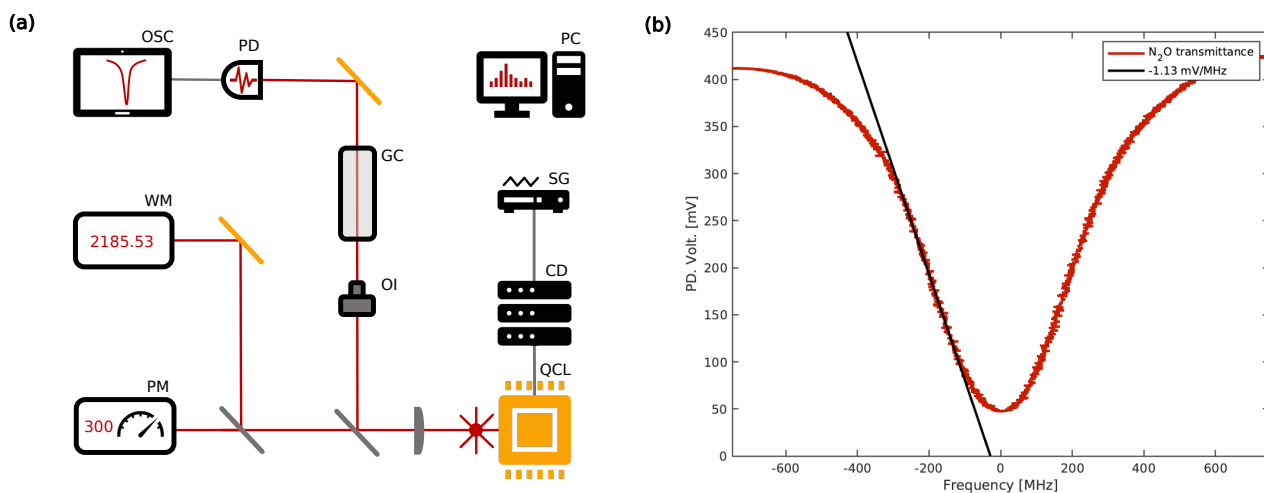


**Figure 3.** (a) Schematic of the experimental setup for characterizing the laser linewidth. The QCL was controlled by a current driver (CD) which was modulated by a triangular waveform from a signal generator (SG). Radiation from the QCL passed through an optical isolator (OI) and a gas cell (GC) filled with N<sub>2</sub>O. The transmitted laser intensity was measured on an infrared-sensitive HgCdTe photodetector (PD) allowing the observation of absorption lines of N<sub>2</sub>O on an oscilloscope (OSC). A part of the laser light was split off and diverted to a wavemeter (WM) and a powermeter (PM). A computer (PC) controlled the experiment and was used to compute the FNPSD. (b) Transmittance signal as a function of the frequency detuning from the laser set point of 2185.53 cm<sup>-1</sup>. The fit of a straight line to the linear region of the slope of the absorption line (black) yields a signal-to-frequency transfer factor of 1.13 mV/MHz.

The FNPSD was obtained from a Fourier transform of the time-dependent transmittance as shown in the red trace in Figure 4. A linewidth of 1.3 MHz was obtained by integrating the area of the FNPSD bounded by the beta separation line Equation (2), shown as the black line in Figure 4 [29], for an observation time of 10 ms. This observation time was chosen to cover broad area of the spectrum, abandoning only low frequency noise less than 100 Hz.

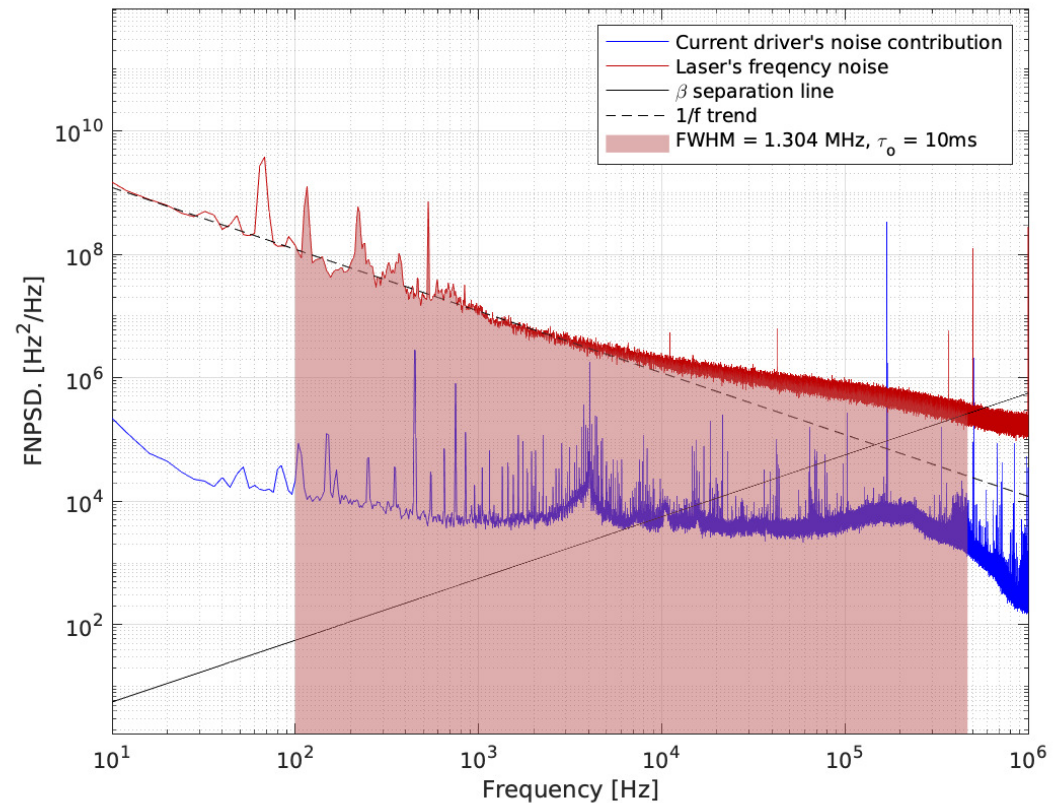


**Figure 4.** The frequency noise power spectral density (FNPSD) of the laser (red trace) follows a  $1/f$  trend up to 2 kHz. The contribution of the current driver (blue trace) to the frequency noise is negligible. The FNPSD of the laser is crossed by the beta separation line at 467 kHz resulting in a laser linewidth equal to 1.3 MHz for an observation time  $\tau_o = 10$  ms. The operation current and temperature of the laser were set to 650 mA and  $-20$  °C during the FNPSD measurement.

Moreover, to verify that the measured linewidth was not limited by the contribution of the laser current driver to the FNPSD, we measured the current noise on a shielded high-precision 10 Ohm resistor as a function of time. These data were converted into a FNPSD by Fourier transform and applying the current-to-frequency conversion factor of 0.36 GHz/mA for the present laser. This conversion factor was obtained from a linear fit of the laser frequency measured as a function of the driver current which was calibrated by comparison to a simulated  $N_2O$  absorption spectrum based on spectroscopic data retrieved from the HITRAN database [30].

### 3. Discussion

From the FNPSD of the laser in Figure 4, it can be seen that in the low-frequency region up to 1 kHz, flicker noise dominates, affecting the frequency noise. This effect, typical for QCLs, was attributed to fluctuations of electrons tunnelling through the multi-barrier structure, which in turn induce temperature fluctuations contributing to noise [31].

The QCL frequency noise decreases less steeply than the  $1/f$  trend (black dashed line in Figure 4) above  $\sim 2$  kHz. This behaviour is reminiscent of noise induced by current-density fluctuations affecting the semiconductor-laser temperature. However, because this process is strongly suppressed in QCLs [17], this contribution to the noise spectrum could also be caused by external temperature fluctuations due to the open housing of the laser.

The present QCL was mounted epi-side up, i.e., it was soldered in the same direction as the growth of the active region, in a non-sealed homemade housing. Nitrogen purge gas was constantly used to prevent condensation of ambient moisture inside the housing at the working temperature of the device of  $-20$  °C in this study. This nitrogen flow led to an instability of the laser temperature resulting in additional frequency noise. To further reduce the influence of the environment on the laser linewidth, one could consider mounting the laser epi-side down for a better thermal management and place the device in a sealed housing which should result in a lower linewidth for a similarly free-running device.

From Figure 4, one can see that the contribution of the current driver to the laser frequency noise is orders of magnitude smaller than the noise of the detector and, therefore, is negligible.

The measured device shows a twice higher output power than the most powerful narrow-linewidth dual-mode QCL reported so far to our knowledge [32] (see Figure 5 and Table 1). Figure 5 shows the output power of the devices reported in the literature in Table 1 as a function of the ratio between the FWHM and the emitted frequency of the device enabling a direct comparison of the linewidth across different emission wavelength ranges. The free-running linewidth of the QCL presented here should be sufficiently narrow for a tight lock of the laser to achieve a further linewidth reduction. For instance, the high power of the present device should enable a non-linear frequency conversion to the near IR region in order to lock the laser to a frequency comb [6].

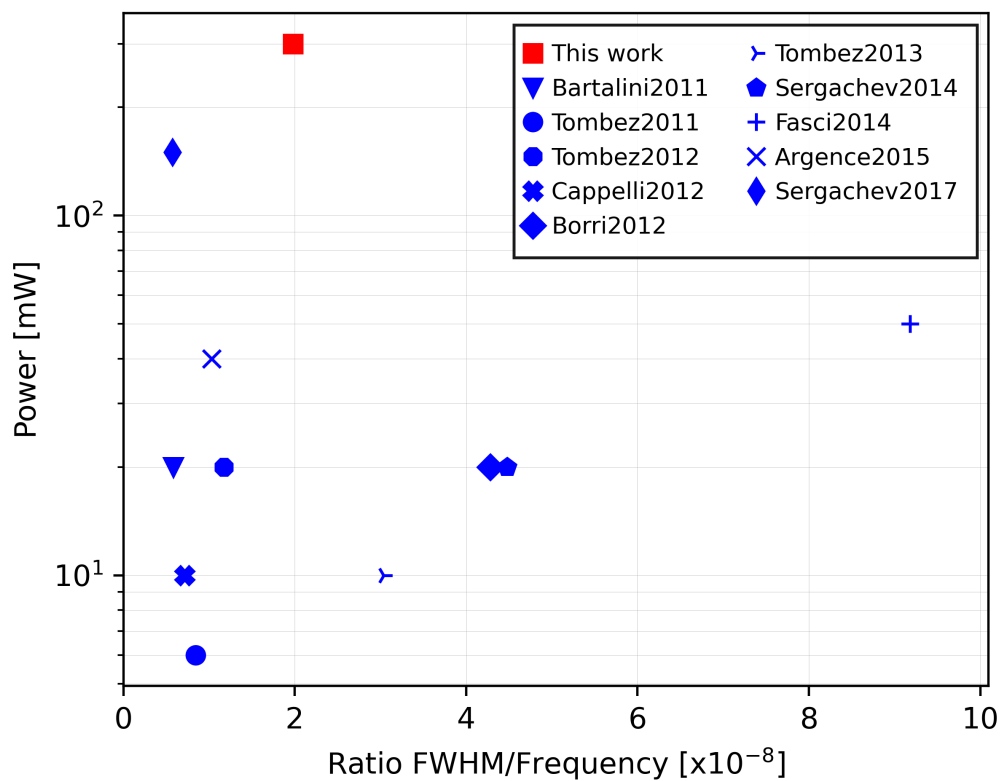


**Figure 5.** Maximum output powers as a function of the ratio of the FWHM with the emitted frequency of free-running narrow linewidth QCLs reported since 2010.

**Table 1.** Maximum output powers, free-running linewidths (full width at half maximum, FWHM), observation times and central wavelengths (WL) of free-running narrow linewidth QCLs reported in the literature since 2010.

Current State of the Art					
Pow. [mW]	FWHM [kHz]	Obs. Time [ms]	WL [ $\mu\text{m}$ ]	Author	Ref.
>300	1300	10	4.56	Bertrand 2022	this work
20	400	10	4.36	Bartalini 2011	[33]
6	550	5	4.6	Tombez 2011	[8]
20	770	10	4.56	Tombez 2012	[34]
10	500	1	4.3	Cappelli 2012	[35]
20	2750	50	4.67	Borri 2012	[36]
10	2000	10	4.55	Tombez 2013	[37]
20	1700	10	7.9	Sergachev 2014	[38]
50	3200	1	8.6	Fasci 2014	[39]
40	300	1000	10.3	Argence 2015	[6]
150	380	1	4.5	Sergachev 2017	[32]

#### 4. Outlook

We reported the development and characterization of a high-power single-mode narrow-linewidth mid-IR QCL. The MOPA technique employed allowed us to produce a device emitting more than 300 mW at 4.6  $\mu\text{m}$  in continuous operation with a linewidth of 1.3 MHz. The output power obtained exceeds the previously reported single-mode lasers by about a factor of two. The present device is an ideal tool for, e.g., precision spectroscopy of dipole-forbidden transitions in molecules for which high laser intensities are crucial [18].

**Author Contributions:** Conceptualization, J.F., S.W. and M.B. (Mathieu Bertrand); methodology, M.B. (Mathieu Bertrand), A.S. and M.S.; investigation, M.S., A.S., M.B. (Mattias Beck) and M.B. (Mathieu Bertrand); writing—original draft preparation, M.B. (Mathieu Bertrand) and A.S.; writing—review and editing, M.B. (Mathieu Bertrand), A.S., S.W. and J.F.; funding acquisition, S.W. and J.F. All authors have read and agreed to the published version of the manuscript.

**Funding:** We acknowledge financial support from the Swiss National Science Foundation as part of the National Centre of Competence in Research, Quantum Science and Technology (NCCR-QSIT) and grant nr. CRSII5 183579.

**Institutional Review Board Statement:** Not applicable.

**Informed Consent Statement:** Not applicable.

**Data Availability Statement:** The data can be found at this address: <http://doi.org/10.3929/ethz-b-000564570>.

**Conflicts of Interest:** The authors declare no conflict of interest.

#### Abbreviations

The following abbreviations are used in this manuscript:

QCL	Quantum Cascade Laser
FWHM	Full Width Half Maximum
DFB	Distributed Feedback Bragg Reflector
MOPA	Master Oscillator Power Amplifier
FNSPD	Frequency Noise Power Spectral Density
CW	Continuous Wave



## References

1. Faist, J.; Capasso, F.; Sivco, D.L.; Sirtori, C.; Hutchinson, A.L.; Cho, A.Y. Quantum Cascade Laser. *Science* **1994**, *264*, 553. [[CrossRef](#)] [[PubMed](#)]
2. Santagata, R.; Tran, D.B.A.; Argence, B.; Lopez, O.; Tokunaga, S.K.; Wiotte, F.; Mouhamad, H.; Goncharov, A.; Abgrall, M.; Coq, Y.L.; et al. High-precision methanol spectroscopy with a widely tunable SI-traceable frequency-comb-based mid-infrared QCL. *Optica* **2019**, *6*, 411. [[CrossRef](#)]
3. Genner, A.; Martín-Mateos, P.; Moser, H.; Lendl, B. A Quantum Cascade Laser-Based Multi-Gas Sensor for Ambient Air Monitoring. *Sensors* **2020**, *20*, 1850. [[CrossRef](#)] [[PubMed](#)]
4. Krötz, P.; Stupar, D.; Krieg, J.; Sonnabend, G.; Sornig, M.; Giorgetta, F.; Baumann, E.; Giovannini, M.; Hoyler, N.; Hofstetter, D.; et al. Applications for quantum cascade lasers and detectors in mid-infrared high-resolution heterodyne astronom. *Appl. Phys. B* **2008**, *90*, 187. [[CrossRef](#)]
5. Germann, M.; Tong, X.; Willitsch, S. Observation of electric-dipole-forbidden infrared transitions in cold molecular ions. *Nat. Phys.* **2014**, *10*, 820. [[CrossRef](#)]
6. Argence, B.; Chanteau, B.; Lopez, O.; Nicolodi, D.; Abgrall, M.; Chardonnet, C.; Daussey, C.; Darquié, B.; Le Coq, Y.; Amy-Klein, A. Quantum cascade laser frequency stabilization at the sub-Hz level. *Nat. Photonics* **2015**, *9*, 456. [[CrossRef](#)]
7. Myers, T.L.; Williams, R.M.; Taubman, M.S.; Gmachl, C.; Capasso, F.; Sivco, D.L.; Baillargeon, J.N.; Cho, A.Y. Free-running frequency stability of mid-infrared quantum cascade lasers. *Opt. Lett.* **2002**, *27*, 170. [[CrossRef](#)]
8. Tombez, L.; Francesco, J.D.; Schilt, S.; Domenico, G.D.; Faist, J.; Thomann, P.; Hofstetter, D. Frequency noise of free-running 4.6  $\mu\text{m}$  distributed feedback quantum cascade lasers near room temperature. *Opt. Lett.* **2011**, *36*, 3109. [[CrossRef](#)]
9. Razeghi, M.; Slivken, S.; Bai, Y.; Gokden, B.; Darvish, S.R. High power quantum cascade lasers. *New J. Phys.* **2009**, *11*, 125017. [[CrossRef](#)]
10. Bai, Y.; Bandyopadhyay, N.; Tsao, S.; Slivken, S.; Razeghi, M. Room temperature quantum cascade lasers with 27% wall plug efficiency. *Appl. Phys. Lett.* **2011**, *98*, 181102. [[CrossRef](#)]
11. Lyakh, A.; Maulini, R.; Tsekoun, A.; Go, R.; Patel, C.K.N. Multiwatt long wavelength quantum cascade lasers based on high strain composition with 70% injection efficiency. *Opt. Express* **2012**, *20*, 24272. [[CrossRef](#)]
12. Schawlow, A.L.; Townes, C.H. Infrared and Optical Masers. *Phys. Rev.* **1958**, *112*, 1940. [[CrossRef](#)]
13. Henry, C. Theory of the linewidth of semiconductor lasers. *IEEE J. Quantum Electron.* **1982**, *18*, 259. [[CrossRef](#)]
14. Aellen, T.; Maulini, R.; Terazzi, R.; Hoyler, N.; Giovannini, M.; Faist, J.; Blaser, S.; Hvozdar, L. Direct measurement of the linewidth enhancement factor by optical heterodyning of an amplitude-modulated quantum cascade laser. *Appl. Phys. Lett.* **2006**, *89*, 091121. [[CrossRef](#)]
15. Hangauer, A.; Wysocki, G. Gain Compression and Linewidth Enhancement Factor in Mid-IR Quantum Cascade Lasers. *IEEE J. Sel. Top. Quantum Electron.* **2015**, *21*, 74–84. [[CrossRef](#)]
16. Bartalini, S.; Borri, S.; Cancio, P.; Castrillo, A.; Galli, I.; Giusfredi, G.; Mazzotti, D.; Gianfrani, L.; De Natale, P. Observing the Intrinsic Linewidth of a Quantum-Cascade Laser: Beyond the Schawlow-Townes Limit. *Phys. Rev. Lett.* **2010**, *104*, 083904. [[CrossRef](#)]
17. Yamanishi, M.; Edamura, T.; Fujita, K.; Akikusa, N.; Kan, H. Theory of the Intrinsic Linewidth of Quantum-Cascade Lasers: Hidden Reason for the Narrow Linewidth and Line-Broadening by Thermal Photons. *IEEE J. Quantum Electron.* **2008**, *44*, 12. [[CrossRef](#)]
18. Najafian, K.; Meir, Z.; Willitsch, S. From megahertz to terahertz qubits encoded in molecular ions: theoretical analysis of dipole-forbidden spectroscopic transitions in  $\text{N}_2^+$ . *Phys. Chem. Chem. Phys.* **2020**, *22*, 23083. [[CrossRef](#)]
19. Menzel, S.; Diehl, L.; Pflügl, C.; Goyal, A.; Wang, C.; Sanchez, A.; Turner, G.; Capasso, F. Quantum cascade laser master-oscillator power-amplifier with 1.5 W output power at 300 K. *Opt. Express* **2011**, *19*, 16229–16235. [[CrossRef](#)]
20. Hinkov, B.; Beck, M.; Gini, E.; Faist, J. Quantum cascade laser in a master oscillator power amplifier configuration with Watt-level optical output power. *Opt. Express* **2013**, *21*, 19180. [[CrossRef](#)]
21. Faist, J.; Hofstetter, D.; Beck, M.; Aellen, T.; Rochat, M.; Blaser, S. Bound-to-continuum and two-phonon resonance, quantum-cascade lasers for high duty cycle, high-temperature operation. *IEEE J. Quantum Electron.* **2002**, *38*, 533–546. [[CrossRef](#)]
22. Beck, M.; Faist, J.; Oesterle, U.; Illegems, M.; Gini, E.; Melchior, H. Buried heterostructure quantum cascade lasers with a large optical cavity waveguide. *IEEE Photonics Technol. Lett.* **2000**, *12*, 1450–1452. [[CrossRef](#)]
23. Süess, M.J.; Peretti, R.; Liang, Y.; Wolf, J.M.; Bonzon, C.; Hinkov, B.; Nida, S.; Jouy, P.; Metaferia, W.; Lourduoss, S.; et al. Advanced Fabrication of Single-Mode and Multi-Wavelength MIR-QCLs. *Photonics* **2016**, *3*, 26. [[CrossRef](#)]
24. Bertrand, M.; Franckić, M.; Forrer, A.; Faist, J. 2022. *unpublished*.
25. Okoshi, T.; Kikuchi, K.; Nakayama, A. Novel method for high resolution measurement of laser output spectrum. *Electron. Lett.* **1980**, *16*, 630. [[CrossRef](#)]
26. Ludvigsen, H.; Tossavainen, M.; Kaivola, M. Laser linewidth measurements using self-homodyne detection with short delay. *Opt. Commun.* **1998**, *155*, 180. [[CrossRef](#)]
27. Baney, D.M.; Sorin, W.V. *Fiber Optic Test and Measurement*; Chapter 13; Prentice-Hall: Hoboken, NJ, USA, 1998.
28. Bucalovic, N.; Dolgovskiy, V.; Schori, C.; Thomann, P.; Domenico, G.D.; Schilt, S. Experimental validation of a simple approximation to determine the linewidth of a laser from its frequency noise spectrum. *Appl. Opt.* **2012**, *51*, 4582. [[CrossRef](#)] [[PubMed](#)]

29. Domenico, G.D.; Schilt, S.; Thomann, P. Simple approach to the relation between laser frequency noise and laser line shape. *Appl. Opt.* **2010**, *49*, 4801. [[CrossRef](#)]
30. Gordon, I.; Rothman, L.; Hargreaves, R.; Hashemi, R.; Karlovets, E.; Skinner, F.; Conway, E.; Hill, C.; Kochanov, R.; Tan, Y.; et al. The HITRAN2020 molecular spectroscopic database. *J. Quant. Spectrosc. Radiat. Transf.* **2022**, *277*, 107949. [[CrossRef](#)]
31. Borri, S.; Bartalini, S.; Pastor, P.C.; Galli, I.; Giusfredi, G.; Mazzotti, D.; Yamanishi, M.; De Natale, P. Frequency-Noise Dynamics of Mid-Infrared Quantum Cascade Lasers. *IEEE J. Quantum Electron.* **2011**, *47*, 984. [[CrossRef](#)]
32. Sergachev, I.; Maulini, R.; Gresch, T.; Blaser, S.; Bismuto, A.; Müller, A.; Bidaux, Y.; Südmeyer, T.; Schilt, S. Frequency stability of a dual wavelength quantum cascade laser. *Opt. Express* **2017**, *25*, 11027. [[CrossRef](#)]
33. Bartalini, S.; Borri, S.; Galli, I.; Giusfredi, G.; Mazzotti, D.; Edamura, T.; Akikusa, N.; Yamanishi, M.; Natale, P.D. Measuring frequency noise and intrinsic linewidth of a room-temperature DFB quantum cascade laser. *Opt. Express* **2011**, *19*, 17996. [[CrossRef](#)] [[PubMed](#)]
34. Tombez, L.; Schilt, S.; Francesco, J.D.; Thomann, P.; Hofstetter, D. Temperature dependence of the frequency noise in a mid-IR DFB quantum cascade laser from cryogenic to room temperature. *Opt. Express* **2012**, *20*, 6851. [[CrossRef](#)] [[PubMed](#)]
35. Cappelli, F.; Galli, I.; Borri, S.; Giusfredi, G.; Cancio, P.; Mazzotti, D.; Montori, A.; Akikusa, N.; Yamanishi, M.; Bartalini, S.; et al. Subkilohertz linewidth room-temperature mid-infrared quantum cascade laser using a molecular sub-Doppler reference. *Opt. Lett.* **2012**, *37*, 4811. [[CrossRef](#)] [[PubMed](#)]
36. Borri, S.; Galli, I.; Cappelli, F.; Bismuto, A.; Bartalini, S.; Cancio, P.; Giusfredi, G.; Mazzotti, D.; Faist, J.; Natale, P.D. Direct link of a mid-infrared QCL to a frequency comb by optical injection. *Opt. Lett.* **2012**, *37*, 1011. [[CrossRef](#)]
37. Tombez, L.; Schilt, S.; Hofstetter, D.; Südmeyer, T. Active linewidth-narrowing of a mid-infrared quantum cascade laser without optical reference. *Opt. Lett.* **2013**, *38*, 5079. [[CrossRef](#)]
38. Sergachev, I.; Maulini, R.; Bismuto, A.; Blaser, S.; Gresch, T.; Bidaux, Y.; Müller, A.; Schilt, S.; Südmeyer, T. All-electrical frequency noise reduction and linewidth narrowing in quantum cascade lasers. *Opt. Lett.* **2014**, *39*, 6411. [[CrossRef](#)]
39. Fasci, E.; Coluccelli, N.; Cassinerio, M.; Gambetta, A.; Hilico, L.; Gianfrani, L.; Laporta, P.; Castrillo, A.; Galzerano, G. Narrow-linewidth quantum cascade laser at 8.6  $\mu\text{m}$ . *Opt. Lett.* **2014**, *39*, 4946. [[CrossRef](#)]